

# Fouling and biofouling resistance of metal-doped mesostructured silica/polyethersulfone ultrafiltration membranes

This version is made available in accordance with publisher policies.

Please, cite as follows:

Berta Díez, Nuria Roldán, Antonio Martín, Arcadio Sotto, José Antonio Perdigón-Melón, Jesús Arsuaga, Roberto Rosal, Fouling and biofouling resistance of metal-doped mesostructured silica/polyethersulfone ultrafiltration membranes, *Journal of Membrane Science*, 526, 252–263, 2017, <http://dx.doi.org/10.1016/j.memsci.2016.12.051>.

# Fouling and biofouling resistance of metal-doped mesostructured silica/polyethersulfone ultrafiltration membranes

Berta Díez<sup>1</sup>, Nuria Roldán<sup>2</sup>, Antonio Martín<sup>2</sup>, Arcadio Sotto<sup>2</sup>, José Antonio Perdigón-Melón<sup>1</sup>, Jesús Arsuaga<sup>2,\*</sup>, Roberto Rosal<sup>1,\*</sup>

1 Department of Chemical Engineering, University of Alcalá, E-28871 Alcalá de Henares, Madrid, Spain

2 School of Experimental Science and Technology, ESCET, Rey Juan Carlos University, E-28933, Móstoles, Madrid, Spain

\* Corresponding authors: [jesusmaria.arsuaga@urjc.es](mailto:jesusmaria.arsuaga@urjc.es), [roberto.rosal@uah.es](mailto:roberto.rosal@uah.es)

## Abstract

Hybrid polyethersulfone-based ultrafiltration membranes were prepared by incorporating metal (Ag and Cu) and/or amine-functionalized mesostructured SBA-15 silica particles. The doping particles were included into the casting solution to obtain a total solids load of 3.6 wt% in the final membranes. The physicochemical characterization of particles and membranes showed a good dispersion of metals inside the mesoporous structure of silica as well as a reduced skin layer, higher pore interconnectivity, and a larger amount of pores in membranes doped with the hydrophilic fillers. Membrane surface was also slightly less hydrophobic in hybrid membranes. Membrane performance was significantly improved as result of considerable increase of water permeation without affect negatively the membrane selectivity. The organic antifouling properties were enhanced with significant permeability improvement without compromising membrane rejection performance. In addition to it, metal-loaded silica allowed preparing membranes with high antibacterial activity. The removal of colonies of *Escherichia coli* and *Staphylococcus aureus* was complete either on membrane surface or in the liquid in contact with membranes when exposed to a 1/500 nutrient broth medium for 20 h at 36 °C. The rate of metal release depended on metal speciation and represented a 0.1–0.6% of the total metal content of membranes.

**Keywords:** hybrid membranes; ultrafiltration; polyethersulfone; organic fouling; biofouling; antimicrobial materials.

## 1. Introduction

Ultrafiltration (UF) is a pressure-driven membrane process widely used for the removal of colloidal/particulate matter, pathogenic microorganisms, and oil-water emulsions [1] and [2]. Polyethersulfone (PES) is a thermoplastic polymer extensively used for the fabrication of UF membranes due to its high mechanical strength besides chemical and thermal stabilities [3]. It is well dissolvable in many aprotic polar solvents, as *N*-Methyl-2-pyrrolidone, and can properly be processed into a porous membrane through the non-solvent induced phase method. Despite these advantages, PES material is not enough hydrophilic and water permeability of PES membranes can become insufficient. In addition, the adsorption and deposition of hydrophobic nonpolar solutes on neat PES membranes surface and inside membrane pores leads to serious decrease in permeation flux and the change in separation characteristic during filtration operation that limits the practical application of PES UF membranes [4]. The adsorption of unwanted materials onto membrane surface results in a higher energy demand, shorter membrane lifetime and poorer separation performance [5]. Since membrane fouling is a consequence of the interaction between membrane surfaces and solutes by different mechanisms and

hydrophobic interaction is usually accepted as predominant for PES membranes, the dispersion component of surface tension could be a good fouling predictor [6] and [7]. Many attempts have been performed to improve the fouling resistance of PES membranes by surface modifications, which include grafting, coating or different surface functionalization treatments with the aim of obtaining enhanced hydrophilicity or biocompatibility [8]. The use of blending additives following surface functionalization has also been successfully explored [9].

Biofouling is another major problem for the application of PES UF membranes. The biofouling is due to cells with altered phenotype that attach and grow on membrane surface forming complex biological communities [10]. Biofilms create their own environment and, once formed, are very difficult to remove often causing permanent permeability loss and irreversible membrane damage [11]. The enhancement of surface hydrophilicity has been extensively explored for preparing low biofouling PES membranes. Blends with hydrophilic polymers and the inclusion of different nanoparticles have been proposed for biofouling prevention [12] and [13]. Also, the use of metal nanoparticles has been frequently reported in view of the toxicity of certain metals against a variety of

microorganisms including bacteria and fungi. Metals can cause oxidative stress, directly or by inactivating the cellular mechanisms normally involved in quenching reactive oxygen species [14]. It has been shown that silver, copper and other metals induce oxidative stress followed by membrane disruption, interference in enzymatic functions, among others [15]. Thanks to it, silver and copper as salts or nanoparticles have been proposed for a number of antimicrobial materials [16] and [17].

The incorporation of many diverse types of nanomaterials within the polymer matrix have been proposed for preparing hybrid UF membranes, which include silica, free metals and metal oxides, among others [18] and [19]. Particularly, mesoporous silica has been investigated for the preparation of mixed matrix ultrafiltration membranes, which benefit from its hydrophilic and porous nature to improve membrane performance. Mesoporous silica has been shown to enlarge pore size, improve pore interconnectivity and increase hydrophilicity and thermal stability with respect to neat PES, thus providing higher flux and better antifouling performance [20]. Mesoporous silica particles functionalized with amino and carboxylic groups have been studied for enhancing antifouling performance with significant improvements in water permeability, surface porosity, hydrophilicity, and stability [21]. Otherwise, nanometals, particularly silver, have been extensively studied for membrane nanocomposites [22]. Apart from production costs, the incorporation of nanoparticles into polymeric membranes has two important drawbacks. One is the difficulty of getting a good dispersion of nanoparticles within the polymeric matrix. The other is the possibility of releasing engineered nanomaterials into the environment. Nanometals supported on silica particles or silicates have been proposed to overcome these limitations by preparing stable materials that avoid the dispersion of nanoparticles into the environment [23].

In this work, we prepared new composite polymeric PES ultrafiltration membranes with amino and metal-loaded mesoporous silica as modifying additive incorporated at low weight proportion (less than 4%). The purpose was to obtain UF membranes with mechanical properties similar to those of neat PES, but higher flux, lower organic fouling, and an improved resistance to microbial growth. To prove the latter, several bioassays have been performed using the bacteria *Escherichia coli* and *Staphylococcus aureus* as model microorganisms.

The inclusion of metals in fillers, rather than their direct dispersion into the polymeric solution or their attachment to membrane was intended to avoid the dispersion of nanoforms into the environment. The purpose was to obtain membranes with higher flux and lower fouling, in which metal-loaded mesoporous silica could act as a vehicle for introducing nanometals without the problems derived from particle aggregation,

chemical incompatibility with casting solvents and unintended nanoparticle release. The antimicrobial behavior was tested using the bacteria *Escherichia coli* and *Staphylococcus aureus* as model microorganisms. To the best of our knowledge, this combination of doping mesoporous silica nanoparticles (amino and metal-loaded) planned to enhance water permeability and mitigate both organic fouling and biofouling of PES membranes has not been previously reported.

## 2. Experimental

### 2.1. Materials

Polyethersulfone (PES, 58 kDa) was provided by Solvay Chemicals International (Belgium), and *N*-Methyl-2-pyrrolidone (NMP) was supplied by Scharlau (Barcelona, Spain). Pluronic P123 (Sigma-Aldrich EO<sub>20</sub>PO<sub>70</sub>EO<sub>20</sub>, EO ethylene oxide, PO propylene oxide, MW = 5800), tetraethylorthosilicate (TEOS 98% Sigma-Aldrich), *N*-(3-trimethoxysilylpropyl) diethylenetriamine (97% Sigma-Aldrich), cupric nitrate trihydrate (Fluka) and silver nitrate (Sigma-Aldrich) were used as received. Bovine Serum Albumin (BSA) was purchased from Sigma-Aldrich. The components of culture media were biological grade acquired from Conda-Pronadisa (Spain). Ultrapure water was generated from a Direct-Q™ 5 Ultrapure Water Systems from Millipore (Bedford, MA, USA) with a specific resistance of 18.2 MΩ cm.

Pure SBA-15 sample was synthesized according to a procedure based on triblock copolymer Pluronic P123 as template and TEOS as a source of silica [24]. During a typical synthesis, 4 g of Pluronic were dissolved in 125 mL aqueous HCl 1.9 M at room temperature. After complete dissolution, TEOS was added and the mixture stirred 20 h at 40 °C. The suspension was then transferred to a tightly closed vessel and kept for 24 h at 110 °C without stirring. The obtained white solid was filtered and washed repeatedly with deionized water. The air-dry white powder was next calcined at 550 °C for 5 h (heating rate 1.8 °C min<sup>-1</sup>). Amine-functionalized SBA-15 was prepared by co-condensation method using the same procedure except for the addition of 1.8 g of *N*-(3-trimethoxysilylpropyl) diethylenetriamine 1 h after adding the silica source (TEOS). In this case, the surfactant template was removed by refluxing with ethanol (1 g of sample in 100 mL of ethanol) for 24 h. Amine-functionalized SBA-15 material was referred to as Triamine/SBA-15 in what follows.

The metallic impregnation of SBA-15 was carried out by the minimum volume method. Copper or silver nitrate were dissolved in 30 mL of water. The solution was slowly poured over calcined SBA-15 while stirring. The solid was dried at 50 °C overnight and calcined under airflow for 8 h at 500 °C with the same heating ramp of 1 °C min<sup>-1</sup>. Metal-loaded mesoporous materials, CuO/SBA-15 and Ag/SBA-15, had a content

of 8.9 wt% copper (11.2 wt% as CuO) and 3.5 wt% silver (as Ag). The particle size of SBA-15 and metal-loaded SBA-15 was measured by DLS in polymer solvent medium. The results are shown in Table S1 (in Supplementary Material, SM).

Nitrogen adsorption and desorption isotherms at 77 K were measured using a Micromeritics TRISTAR 3000 system. The data were analysed using the BJH and BET models and the pore total volume ( $V_t$ ) was assigned at  $P/P_0 = 0.975$  as single point. X-ray powder diffraction (XRD) patterns were acquired on a PHILIPS X'PERT diffractometer using Cu K $\alpha$  radiation. The data were recorded from 0.5 to 5° (2 $\theta$ ). Transmission electron microscopy (TEM) microphotographs were carried out on a PHILIPS TECNAI-20 electronic microscope operating at 200 kV.

## 2.2. Membrane preparation and characterization

Membranes were prepared using non-solvent induced phase inversion by means of immersion/precipitation with PES cast from a solution containing 16 wt% of polymer in NMP. Hybrid membranes were prepared by incorporating SBA-15 (pure, amine-functionalized, or metal-loaded) to NMP with the help of ultrasonic dispersion for 45 min at 40 °C. Subsequently, the polymer was added to the suspension and stirred for at least 24 h at room temperature and allowed aging for at least 24 h. The amount of incorporated particles was that required to obtain 0.6% wt% in the polymer synthesis mixture. After forming a homogenous solution, the films were casted with 200  $\mu$ m thickness using a filmograph on nonwoven polyester as support layer. The prepared films were immersed in a non-solvent bath (distilled water at 25 °C) for precipitation. The membranes were then transferred into another container with fresh ultrapure water and soaked for 24 h before testing. For each polymer solution composition, several identical membrane sheets were made in order to repeatedly test the water flux and solute rejection. Table 1 summarizes the composition and particle concentration of casting solutions used in this study along with the nomenclature proposed to differentiate the tested membranes.

The morphology of membrane cross-section was observed under Scanning Electron Microscopy (SEM, XL-30 Philips). Due to the image magnification required to observe the membrane surface porosity, a Field Emission Gun Scanning Electron Microscope (FEG-SEM, FEI Co.) was used.

Surface  $\zeta$ -potential was measured by electrophoretic light scattering using the Surface Zeta Potential Cell (ZEN 1020) with a Zeta Sizer (DLS, Malvern Zetasizer Nano ZS). A rectangular section of the membranes was inserted in a dispensable plastic cuvette containing 10 mM KCl aqueous solution with 0.5% (w/w) polyacrylic acid (450 kDa) as negative-tracer, pH was adjusted at 7.0. Measurements were conducted at 25 °C at six different displacements from the sample surface to

calculate the surface  $\zeta$ -potential. The experimental data are shown in Table S2 (SM).

**Table 1.** Membranes prepared in this investigation

Membrane	Filler content (wt%)	Nomenclature
PES	–	PES
PES/SBA-15	SBA-15 (0.6)	SBA@PES
PES/(Triamine/SBA-15)	Triamine/SBA-15 (0.6)	TriSBA@PES
PES/(Ag/SBA-15)	Ag/SBA-15 (0.6)	AgSBA@PES
PES/(Cu/SBA-15)	Cu/SBA-15 (0.6)	CuSBA@PES
PES/(Triamine/SBA-15+Ag/SBA-15)	Triamine/SBA-15(0.3)+Ag/SBA-15(0.3)	AgTriSBA@PES
PES/(Triamine/SBA-15+Cu/SBA-15)	Triamine/SBA-15(0.3)+Cu/SBA-15(0.3)	CuTriSBA@PES

The Surface free energy was determined by measuring contact angles (CA) with water (Milli-Q), glycerol, and diiodomethane using an optical contact angle meter (Krüss DSA25 Drop Shape Analysis System) operating at room temperature. The components of the surface tension were estimated according to the procedure described in Supplementary Material expression [25] and [26]. The procedure allowed obtaining the free energy of interaction between two identical surfaces immersed in a liquid,  $\Delta G_{SLS}$ , which gives a measure of the hydrophobicity or hydrophilicity of the surface. If  $\Delta G_{SLS} > 0$ , the surface is hydrophilic, and if  $\Delta G_{SLS} < 0$ , it is hydrophobic. The results of this calculation are shown in Table S2 (SM). Prior to contact angle measurements, membranes specimens were vacuum-dried at 90 °C for 2 hours. In the case of bacterial contact angles, measurements were performed on bacterial lawns deposited on cellulose acetate filters an initial concentration of 108 cells/mL. Each measurement was performed in triplicate using the sessile drop technique.

ICP-MS analyses of metal released from membranes were performed on an ICP-MS model X Serie 2 system apparatus from Thermo Scientific. Membranes were submerged in 15 mL of ultrapure water in glass bottles for 24 h in static runs performed at 25 °C. In order to assess the unintended release of nanometals, representative samples of the filtrate recovered after prescribed cumulative times (30, 60, 90 and 120 min) were further ultrafiltrated using Vivaspin 20, 5 kDa, PES centrifuge tubes. The samples were analysed for metals using ICP-MS. In case of nanoparticle release, the amount of metals detected by ICP-MS in the 5 kDa ultrafiltrates would be significantly lower than that of membrane permeate as 5 kDa filters retain particles larger than 2 nm. TMP was set at 2 bar and three replicates of all assays were performed.

## 2.3. Filtration studies

Filtration experiments were carried out by using a crossflow cell module with an effective membrane area of 50 cm<sup>2</sup> connected to a 2 L volume tank. The membrane permeation flux for pure water was

determined in a filtration recycle mode at 2 bar, and 0.65 m s<sup>-1</sup> crossflow velocity. Previously, the linear behavior of water flux against transmembrane pressure (TMP) was confirmed in the 1–4 bar range. Fresh prepared membranes were initially compacted for 2 h at 4 bar and 25 °C.

Membrane fouling was studied by using BSA as organic foulant following the protocol reported elsewhere with BSA solution (1 g L<sup>-1</sup>, pH 7.2) in 0.1 M phosphate-buffered physiological saline (PBS) [27]. To explore the effect of fouling on the membrane permeation performance, pure water and BSA solution filtration experiments were successively performed at 2 bar TMP and fouling was evaluated through pure water flux ratio as expressed by Eq. (1):

$$\text{Flux ratio (\%)} = \left( \frac{J_w^f}{J_w^i} \right) \times 100 \quad (1)$$

where pure water flux was measured before filtration of the BSA solution ( $J_w^i$ ) and after stabilization of the BSA solution flow ( $J_w^f$ ), being the membrane repeatedly washed with distilled water preceding the pure water flux measurement.

Solute rejection,  $R(\%)$ , was evaluated from aqueous solutions of BSA (1 g L<sup>-1</sup>). The permeate ( $C_p$ ) and feed ( $C_f$ ) concentrations of BSA were measured by using a Cary 5000 UV–Vis–NIR Spectrophotometer and compared to determine rejection as follows:

$$R(\%) = \left( 1 - \frac{C_p}{C_f} \right) \times 100 \quad (2)$$

For each polymer solution composition, not less than five filtration essays with different membrane samples were made until obtaining reproducible values of flux and solute rejection.

## 2.4. Microbiological assays

The microorganisms used in these studies were *Escherichia coli* (CETC 516) and *Staphylococcus aureus* (CETC 240). *E. coli* and *S. aureus* are gram-negative and gram-positive strains, respectively, recommended as testing microorganism in the ISO 22196 in order to measure the antibacterial activity on plastic surfaces [28]. The bacteria were maintained at -80 °C in glycerol (20% v/v) until use. Reactivation was performed using NB nutrient broth culture medium (peptone 10 g L<sup>-1</sup>, sodium chloride 5 g L<sup>-1</sup>, meat extract 5 g L<sup>-1</sup> and, in for solid medium, powder agar 15 g L<sup>-1</sup>) at 36 °C. The pH was adjusted to 7.0 ± 0.1. The stationary phase was reached and the optimal density optical (OD) were measured at 600 nm.

The antimicrobial behavior of membranes was tested by counting the CFU (Colonies Forming Units) of *E. coli* and *S. aureus* under the standardized conditions of the

ISO 22196 test, followed with minor modifications. The initial bacterial concentration was set as 10<sup>6</sup> cells/mL inoculated into sterile 24-well microplates. The volume of inoculum was established at 0.15 mL/mg of membrane. Culture time was 20 h ± 1 h at 36 °C, which was enough to form biofilms on non-modified membranes. The culture conditions ensured that bacteria were cultured in their exponential growth phase without nutrient limitation. After incubation, bacterial suspensions and cells detached from membranes were serially diluted to perform CFU counting. For liquid cultures, 10-fold serial dilutions were performed in PBS following which 10 µL were spot-plated on solid agar. In accordance to the ISO 22196 protocol bacteria were recovered from membrane surface by using 2 mL soybean-casein-digest-lecithin-polyoxyethylene sorbitan monooleate (SCDLP broth). Previously membranes were rinsed with PBS for 30 min in an orbital shaker. SCDLP liquid was serially diluted in PBS and spot-plated. The counting was performed in triplicate in three independent runs. Routine analyses were performed to ensure all microbial load was recovered from exposed membranes.

SEM and confocal micrographs of membranes colonized by *E. coli* and *S. aureus* were taken after inoculation with 10<sup>6</sup> cells/mL, 0.15 mL/mg membrane, and incubation in NB medium at 36 °C for 20 ± 1 h. For SEM images, membranes were cleaned with distilled water, fixed, and dehydrated with ethanol and acetone. SEM micrographs were obtained in a ZEISS DSM-950 instrument operating at 25 kV. Live/Dead BacLight Bacterial Viability kit (Molecular Probes, Invitrogen Detection Technologies, Carlsbad, CA, USA) was used to evaluate bacterial viability. This method differentiates viable and no-viability cells using Syto9, a fluorescent nucleic acid stain capable to penetrate cell membrane and bind DNA, and propidium iodide (PI), which is a fluorescent stain marking only membrane-damaged non-viable cells. The excitation/emission maxima were 480/500 nm for Syto9 and 490/635 nm for PI. The micrographs were obtained in a Leica Microsystems Confocal SP5 fluorescence microscope.

## 3. Results and discussion

### 3.1. Particle characterization

Small angle X-ray diffraction patterns of pure, metal-loaded, and amine-functionalized SBA-15 samples are shown in Figure S1 (SM). All diffractograms evidence the presence of mesophases with hexagonal p6mm symmetry, since the characteristic (1 0 0) diffraction peak is clearly distinguished in all the materials [24]. The diffractograms corresponding to pure SBA-15 and the samples in which the functionality was incorporated by post-synthetic procedure (Ag/SBA-15 and Cu/SBA-15) clearly present two additional peaks of plane families (1 1 0) and (2 0 0). The sample synthesized by

co-condensation method, Triamine/SBA-15, also exhibits the same secondary peaks, but very weakly. This fact reflects a reduction of the mesoscopic order due to the structural-distorting phenomena typically observed when the precursors of both mesostructured silica and functionalities are incorporated simultaneously [29].

Nitrogen adsorption-desorption isotherms of the same materials are shown in Figure S2 (SM). All the samples displayed type IV isotherms according to the IUPAC classification, with H1 hysteresis loops characteristic of SBA-15-type mesoporous materials [30]. The sharp change in the adsorbed volume around  $P/P_0 = 0.6-0.8$  in the H1-type hysteresis loop is characteristic of uniform mesopores with open cylindrical geometry [31]. The narrow H1-type hysteresis loop is maintained after the metal incorporation. Consequently, CuO and Ag could penetrate into the porous framework being homogeneously deposited along the cylindrical mesoporous channels. If loaded metal had been placed within the mesoporous structure forming aggregates, it would have provided different wall thicknesses with broader hysteresis loop in the  $N_2$  isotherm [32]. In the case of Triamine/SBA-15 sample, a significant deformation of the hysteresis loop can be appreciated, which could be attributed to the perturbation promoted by amine-organosilane molecules during the silicate condensation process [29]. Table S1 (SM) summarizes the textural properties of the synthesized materials. A decrease in BET surface area,  $S_{BET}$ , and total pore volume,  $V_t$ , is observed for the functionalized samples in comparison with pure SBA-15. The highest reduction was observed for Triamine/SBA-15 where the total pore volume decreased about 35%. This is a common fact when large functionality amount is incorporated by co-condensation route [33]. It should be noted that Cu/SBA-15 and Ag/SBA-15 exhibit pore size values like pure SBA-15 corroborating homogeneous metal deposition into the Mesoporous SBA-15 channels.

Figure S3 (SM) shows TEM images of synthesized samples. SBA-15 internal structure was not modified by the incorporation of functionalities and all the synthesized materials exhibited similar mesoporous ordered patterns in accordance with the XRD results (Figure S1). The pore diameter was graphically estimated around 8 nm for SBA-15, Cu/SBA-15, and Ag/SBA-15 and around 7 nm for Triamine/SBA-15 in fair agreement with values calculated from nitrogen isotherms (Figure S2). Since silver density is much higher than that of  $SiO_2$ , Ag was visible in TEM micrographs as black dots embedded inside the mesoporous channels (Figure S3-C).

### 3.2. Membrane characterization

Cross-sectional images of membranes structure are shown in Fig. 1. PES and modified membranes displayed asymmetric structure with relatively dense skin layer below which finger-like sublayer and porous

substrate were fully developed. However, SBA-15 loaded specimens exhibited morphological changes in both skin layer and finger-like structure sublayer.

Comparing images of neat PES with modified membranes, the presence of enlarged macrovoids is apparent in hybrid membranes. In addition, the skin layer thickness decreased with the presence of particles. Both effects could be explained in terms of faster interdiffusion process (exchange between solvent and non-solvent) during membrane formation as a result of the addition of hydrophilic particles to the ternary thermodynamic system [34]. These morphological changes promote a better pore connectivity throughout the membrane cross-section, which is crucial to the membrane permeation performance. In addition, metal-loaded particles were visible on membrane surface, as shown in AgTriSBA@PES membrane image, which could be act as biofouling inhibitors.

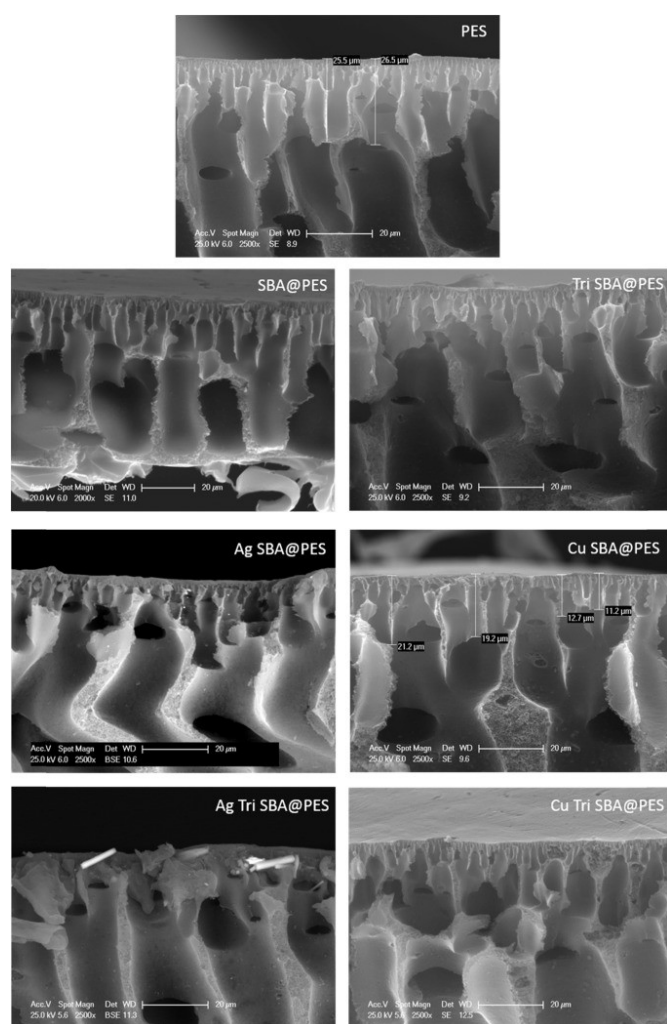


**Figure 1.** Cross-sectional SEM micrographs of membranes manufactured in this investigation.

Comparing images of neat PES with modified membranes, the presence of enlarged macrovoids is apparent in hybrid membranes. In addition, the skin layer thickness decreased with the presence of particles. Both effects could be explained in terms of faster interdiffusion process (exchange between solvent and

non-solvent) during membrane formation because of the addition of hydrophilic particles to the ternary thermodynamic system [34]. These morphological changes promote a better pore connectivity throughout the membrane cross-section, which is crucial to the membrane permeation performance. In addition, metal-loaded particles were visible on membrane surface, as shown in AgTriSBA@PES membrane image, which could be act as biofouling inhibitors.

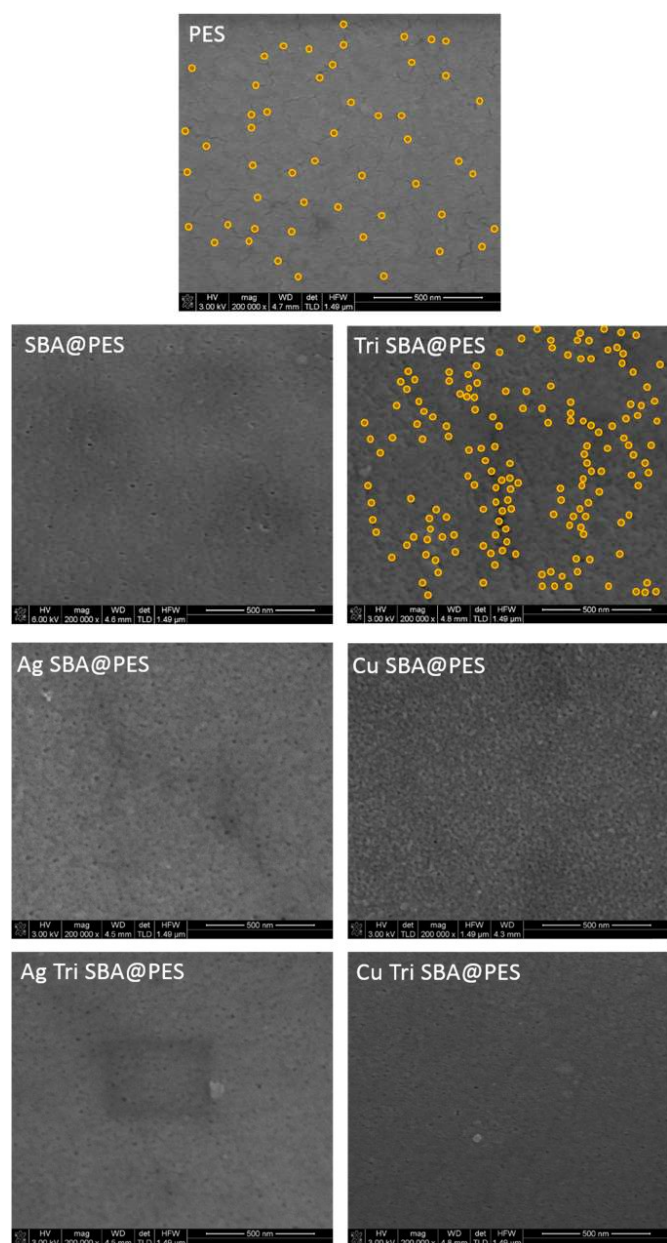


**Figure 2.** FEG-SEM images of manufactured membranes surfaces. Yellow circles have been drawn around pores to facilitate visual interpretation.

The effect of fillers addition on the membrane morphology was also investigated in terms of surface porosity (Fig. 2). The number of pores formed and their spatial distribution onto membrane surface significantly changed because of membrane doping. First, it is apparent that the presence of proposed fillers into the polymeric solution promoted an abrupt formation of new pores: it has been stated that hydrophilic fillers can

act as pore formation agents during the inversion-precipitation process [18]. Second, the pore spatial distribution for neat PES membrane appeared more uniform than that of the doped membrane. Before membrane formation, the dispersion power of solvent determined the spatial configuration of polymer chains inside the polymeric solution. Filler addition reduced the number of polymer chain configurations, promoting the formation of more polymer-lean zones that resulted in nucleation points for pore formation. Besides, the distribution of polymer chains was also affected by the hindrance effect of particles leading to a non-uniform distribution of new pores, because polymer chains can become disrupted in different ways depending on the physicochemical properties of polymer-particle interface [35]. To visualize the enhanced pore formation for modified membranes in comparison with neat PES specimen, yellow circles have been drawn around pores in Fig. 2 for PES and TriSBA@PES samples so remarking the number of formed pores and its spreading on the membrane surface.

The values of the CA for water, glycerol and diiodomethane are shown in Table S2 together with the surface free energy components and the values of  $\Delta G_{SLS}$ . Neat PES membrane was hydrophobic with  $\Delta G_{SLS} \sim -40$  mJ/m<sup>2</sup>, which slightly decreased with the introduction of metal-loaded SBA-15 and, to a higher extent, with amine-functionalized SBA-15. For lawns of *E. coli* and *S. aureus* cells, the surface appeared clearly hydrophilic.

Surface charge measured as surface zeta potential is also shown in Table S2. All membrane surfaces were negatively charged with a zeta potential near -40 mV, except for specimens containing triamine moieties, for which the charge was less negative because of the positive charge imparted by amine moieties at pH 7. The surface  $\zeta$ -potential of prepared membranes was in the -28.3-(-47.6) mV range (in water at pH 7.0), the lowest values corresponding to triamine functionalized membranes.

### 3.3. Filtration performance

The water permeability of neat and modified PES membranes was determined within 1–4 bar TMP range, where flux and pressure displayed a linear relationship demonstrated by exploring the pure water flux over the mentioned range. Permeability was calculated from the slope of the linear correlation between pure water flow and TMP. The results are shown in Fig. 3 from which the enhancement of water permeability against neat PES membrane is apparent for all hybrid membranes. The addition of 0.6 wt. % doping particles resulted in over 30% permeability increase in all cases, which should be explained by the three morphological changes observed in membrane structure because of particle incorporation: enhanced porosity, thinner skin layer, and better pore interconnectivity (Fig. 1). No significant differences between the diverse hybrid

membranes were found, although permeability of SBA@PES sample was systematically lower than membranes containing functionalized SBA-15 nanoparticles. In comparison with previously reported hybrid PES membranes exclusively prepared with amine-functionalized SBA-15 nanoparticles, these new membranes also containing metal-doped mesoporous silica exhibited rather similar permeability values that largely improved the corresponding to neat PES sample. Thus, the expected antimicrobial ability due to silver and copper content was not threatened by water permeability reduction [21].

Since fouling properties of UF membranes were studied by filtering 1 g/L BSA aqueous solutions, rejection experiments were also conducted at 2 bar TMP. Figure S4 (SM) shows the rejection performance found for all the PES prepared membranes, neat and hybrid, calculated from Eq. (2). As observed, the rejection was thoroughly high, above 94%. The incorporation of SBA-15 based materials to polymer matrix barely affected protein retention that even slightly improved for four of the new hybrid membranes.

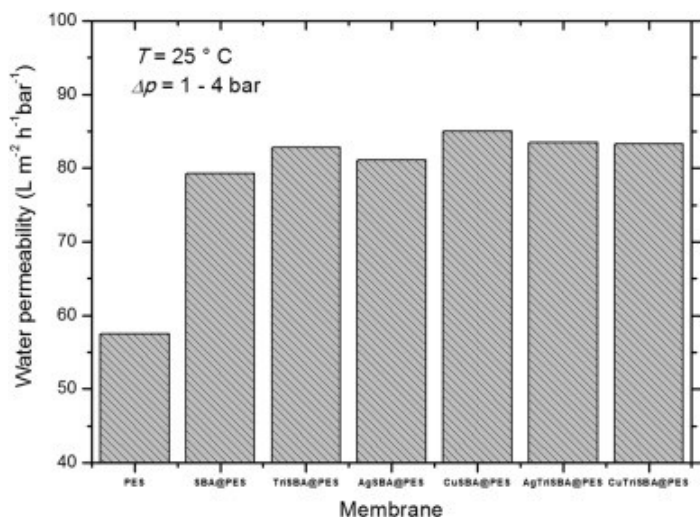


**Figure 3.** Pure water permeability for neat PES and hybrid membranes.

### 3.4. Organic antifouling

The antifouling capacity of membranes was evaluated through pure water flux decline determined before and after filtration of BSA solution. Experiments were initially carried out with perfectly clean specimens; then, the permeate flux of 1 g/L BSA solution at 2 bar was monitored until stabilization; after washing, pure water flux was subsequently obtained. Flux ratios calculated with Eq. (1) are displayed in Fig. 4 that shows how the addition of a small amount (0.6 wt%) of SBA-15 particles to PES membrane reduced fouling between 14 and 29%. Considering that the polymer type and concentration were the same for all membranes, the flux ratio improvement observed for all doped membranes should be exclusively associated to the incorporation of fillers.

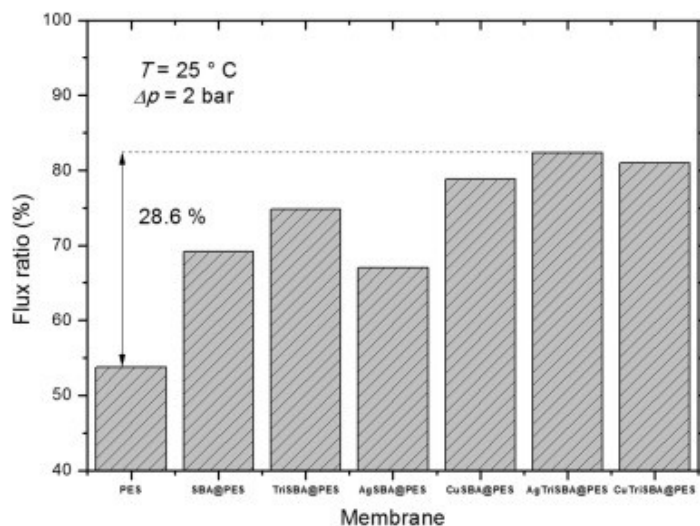


**Figure 4.** Evaluation of irreversible fouling of membranes in terms of pure water flux decline after filtration of 1 g/L BSA solution.

It is expected that protein adsorption on the skin membrane layer and pore plugging could be prevented by increasing surface hydrophilicity due to a high affinity for water as compared to BSA [36]. The addition of hydrophilic fillers should fulfil this goal besides the above mentioned enhancing of macrovoids and pore interconnectivity, which would result in a superior permeability for similar retention properties [22] and [37]. Nevertheless, no strict correlation was found between flux ratio decline and the hydrophilicity (evidences are summarized in Table S2). Water contact angles exhibited no significant differences between the prepared membranes, as expected due to the low nanoparticles content; however, the hydrophilicity estimation from surface free energy (less negative value of  $\Delta G_{SLS}$  refers to more hydrophilic character) revealed an acceptable correspondence to specimens displaying higher flux ratio (e.g., TriSBA@PES and AgTriSBA@PES in Fig. 4).

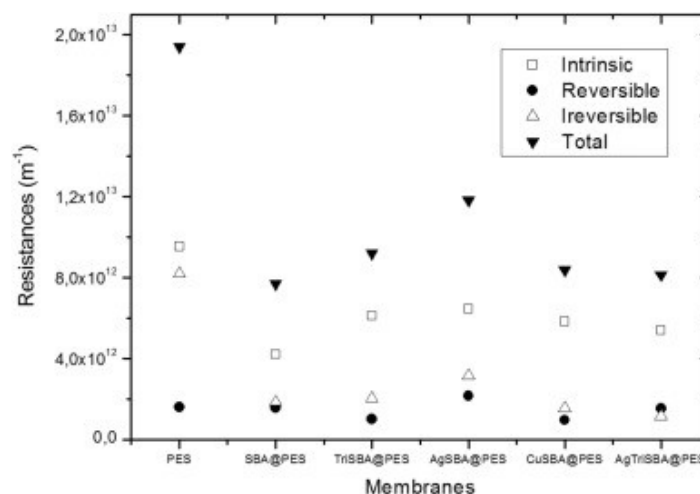


**Figure 5.** Membrane fouling resistances determined from filtration experiments.

To quantitatively describe the fouling resistance for neat and hybrid membranes, the intrinsic, reversible, and irreversible resistances were considered [27]. As observed in Fig. 5, all the calculated resistances for doped membranes were lower than the value corresponding to the neat PES sample. The intrinsic membrane resistance exhibited the dominant contribution to the total membrane resistance in all of tested specimens, suggesting that the membrane permeation is mainly limited by the inherent morphological characteristics of membranes and less influenced by fouling-induced flux restrictions. Reversible resistances were low in all cases and no important difference between neat PES and doped membranes was found.

Conversely, the contribution of irreversible fouling of PES membrane was significantly higher than for hybrid ones. The irreversible adhesion of foulants on membrane surface is recognized as the cause for permanent permeation loss due to the forming of patches around the pores that eventually expand to form a continuous gel layer [38] and [39]. The modification of membranes by embedding metal-doped SBA-15 nanoparticles mitigated the severity of organic fouling over 60% in all tested specimens, as previously found for PES UF hybrid membranes exclusively charged with amine-functionalized mesoporous silica [21].

### 3.5. Antimicrobial behavior

Fig. 6 shows the results of microbial growth tests performed on different membrane specimens exposed to *E. coli* or *S. aureus*. Fig. 6-A refers to colony counting of microorganisms in the 1/500 NB liquid culture in contact with membranes after 20 h of incubation at 36 °C. The growth of *E. coli* and *S. aureus* was not significantly different on SBA@PES, TriSBA@PES and the copper-containing materials CuSBA@PES and CuTriSBA@PES from the control PES membranes. The introduction of silver, either in AgSBA@PES (0.3 wt.% Ag/SBA-15) or in AgTriSBA@PES (0.6 wt.% Ag/SBA-15) resulted in a decrease in the number of viable colonies below the quantification limit of 10 CFU/mL.

The results for microorganisms detached from membrane surface using PBS-SCDLP after removing the culture liquid in contact with them are shown in Fig. 6-B expressed as CFU/cm<sup>2</sup>. There is a higher tendency of *E. coli* to colonize PES membranes with respect to *S. aureus*. *E. coli* and *S. aureus*, being gram-negative and gram-positive bacteria respectively, have quite different bacterial envelopes. Gram-negative bacteria possess an outer membrane and a thin layer of peptidoglycan between this and the cytoplasmic membrane, whereas gram-positive species have a much thicker layer of peptidoglycan [40]. The thick peptidoglycan layer protects bacteria against external stresses including the exposure to toxic metal ions while the outer membrane of gram-negative bacteria possesses porins, which

allow the internalization of ions and low molecular weight substances [41]. The data obtained in this work can be rationalized considering the higher growth rate of *E. coli* respect to *S. aureus* [42]. The number of viable cells recovered from surface decreased for SBA@PES and for TriSBA. In close contact with surface, the copper loaded membranes, CuSBA@PES and CuTriSBA@PES displayed a statistically significant antibacterial action for both bacterial strains with > 50% reduction for TriSBA@PES materials and over 1 log reduction for CuSBA@PES (with double amount of copper). AgSBA@PES and AgTriSBA@PES membrane surfaces were essentially free of bacteria capable of forming new colonies microorganisms, with colony counting below the quantification limit of 1 CFU/cm<sup>2</sup>.

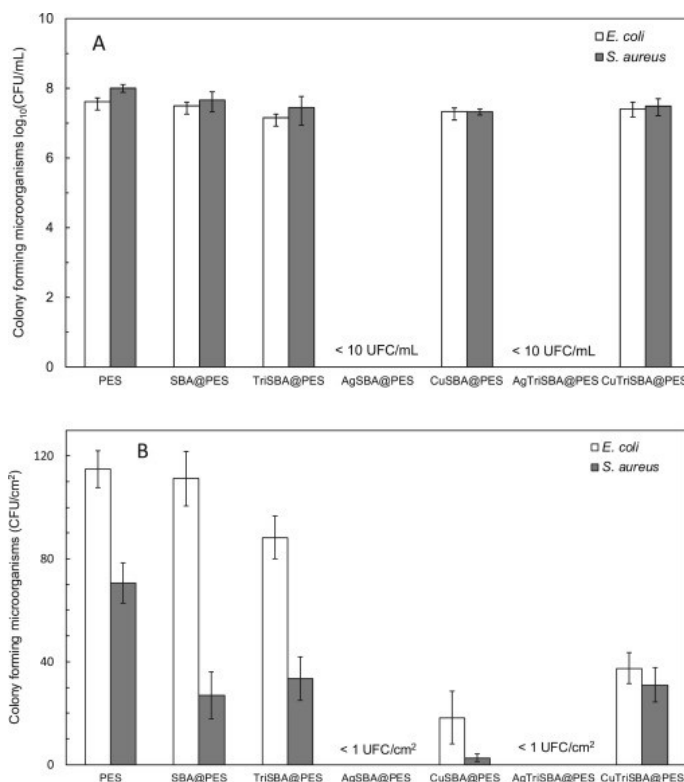


**Figure 6.** Microbial growth for bacterial cultures exposed to membranes (A) and culturable bacteria detached from membranes after incubation (B) at 36 °C, 20 h.

Fig. 7 and S5-S6 (SM) show SEM micrographs of the surface of membranes kept in contact with *E. coli* (Fig. 7) or *S. aureus* (Figure S5) for 20 h at 36 °C following an inoculation of 10<sup>6</sup> cells/mL in NB and the corresponding washing, fixing and drying procedures before imaging. The surface of AgSBA@PES and AgTriSBA@PES membranes appeared almost free of bacteria, only displaying a few cells and scattered objects, probably cell debris. However, PES membranes (Fig. 7 and S5) appeared almost entirely covered by bacteria with already formed biofilm matrix clearly observed. The other non-silver loaded membranes (from which TriSBA@PES is shown in Fig. 7 and S5-S6) displayed certain parts of their

surface relatively clean, while others exhibit a bacterial lawn and evidence of biofilm formation. It must be pointed out that the cultures for Fig. 7 and S5-S6 were obtained after incubation in full NB medium, which is much more favorable for bacterial attachment and colonization than the ISO 22196 1/500 NB used in colony counting experiments.

Figures S7 and S8 (SM) show the results of live/dead bacterial viability staining. The images correspond to representative confocal micrographs of membrane surfaces exposed to *E. coli* (Figure S7) or *S. aureus* (Figure S8) cultures for 20 h at 36 °C in contact with complete NB medium for all membranes but SBA@PES, excluded for simplicity because the micrographs were not significantly different from those of TriSBA@PES. The presence of membrane-damaged bacteria is apparent in all metal loaded specimens (Figures S7 B-C-E-F for *E. coli* and the corresponding images in Figure S8 for *S. aureus*), but also in TriSBA@PES (Figures S7/S8-D) in a slightly higher proportion with respect to control. Figures S7 and S8 show silver-loaded membranes essentially free of viable bacteria, a result in agreement with colony counted performed for membranes in contact with 1/500 NB medium. The presence of red-marked damaged cells was also apparent for CuSBA@PES and CuTriSBA@PES specimens in agreement with the SEM results shown before.

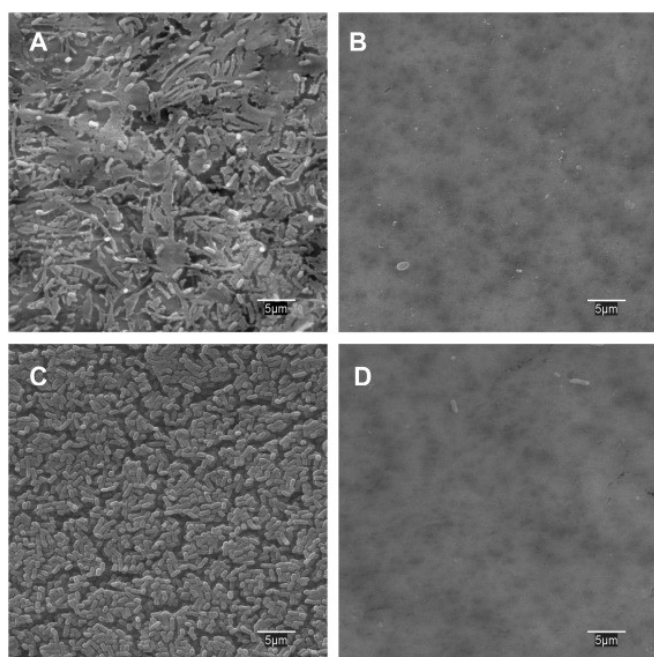


**Figure 7.** Microbial colonization of membranes exposed to *E. coli* cultures (20 h, 36 °C). PES (A), AgSBA@PES (B), TriSBA@PES (C) and AgTriSBA@PES (D).

Hydrophilic bacteria tend to adhere on hydrophilic surfaces but this simple thermodynamic approach assumes direct contact between bacteria and surface and ignores the presence of cell appendages, such as pili and flagella, which makes direct contact a quite unrealistic scenario [43]. The other physicochemical

factor affecting bacterial adhesion is surface charge, which we measured as surface zeta potential (Table S2). All the surfaces of tested membranes were negatively charged and, therefore, electrostatic repulsion is expected to limit bacterial adhesion because of the negative surface charge of bacterial outer membranes. The  $\zeta$ -potential of *E. coli* and *S. aureus* is approximately -40 mV at pH 7 [44]. All the membranes tested in this work displayed similar surface charge, with  $\zeta$ -potential mostly in the -30-(-40) mV range. Consequently, surface charge is not expected to play any significant role in explaining the differential effect observed in this work except for membranes containing triamine-functionalized SBA-15. The data showed a slightly lower tendency to favor the microbial attachment of *E. coli* on membranes containing triamine/SBA-15 in comparison with other metal-free specimens even considering they are more hydrophilic than PES of SBA@PES materials. The reason could be the presence of positively charged domains associated to protonated amines, but the effect is weak. It has been shown that hydrophobicity and charge, while theoretically related to the attachment of different strains, are not good biofouling predictors for most practical situations [45]. Moreover, the surfaces exposed to microbial culture media exhibit complex interfaces with organic and inorganic compounds adsorbed, which modify the way in which microorganisms adhere. More specifically, the free energy of adhesion calculated from surface energy components is strongly affected by the growth medium used for culturing microorganisms, which has a significant impact on bacterial adhesion [46].

Fig. 8 shows the amount of copper and silver released by metal-containing membranes (Cu/AgSBA@PES and Cu/AgTriSBA@PES) after 24 h in water at pH 7 and 20 °C and in 1/500 NB medium. The total amount of silver was 1.26 mg/g of AgSBA@PES membranes (0.63 for AgTriSBA@PES) and that of copper 3.2 mg/g of CuSBA@PES membranes (1.6 for CuTriSBA@PES). This represented 0.1% in water and 0.2% in 1/500 NB medium of the total amount of silver loaded in AgSBA@PES membranes. For copper materials the figures were 0.6% and 0.3% respectively. The amount of silver released was substantially lower in 1/500 NB medium with respect to pure water, with the opposite behavior found for copper materials. The reason for the difference was, most probably, the different speciation of metals, which migrate to the bulk in the form of solvated cations ( $\text{Ag}^+$ ,  $\text{Cu}^{2+}$ ) or as hydroxylated species. Visual MINTEQ (version 3.1, KTH, Stockholm, Sweden) allowed determining that the dominating speciation of copper were  $\text{CuOH}^+$ ,  $\text{Cu}_2(\text{OH})_2^{2+}$  and  $\text{Cu}_3(\text{OH})_4^{2+}$ . In the presence of chloride, the amount of silver released was considerably lower due to the formation of insoluble AgCl. The higher amount of copper detected in solution could be attributed to the interaction with the organic constituents of the culture medium.

The absence of nanoparticle release with membrane filtrate is shown in the results represented in Fig. S9. The content of metals in membrane filtrate and 5 kDa subsequent ultrafiltrate were quantified using the same membranes by ICP-MS. The samples correspond to filtrates recovered during four periods of 30 min following each other. The results show no significant differences between silver and copper concentration before and after 5 kDa filtration, meaning that no nanoparticles higher than 5 kDa membrane pore size (about 2 nm) were present in the filtrate of AgSBA@PES and CuSBA@PES membranes.

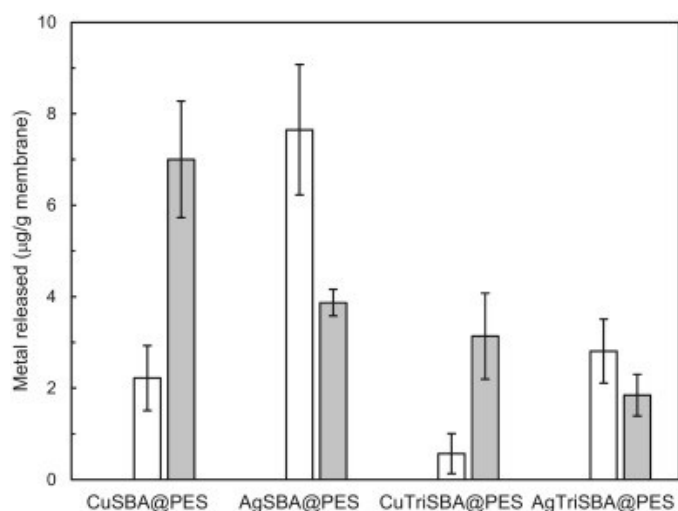


**Figure 8.** Metal released per unit mass of membrane after 20 h in contact with water (empty bars) or NB 1/500 culture medium (grey bars).

The antibacterial effect of silver materials in cases in which silver nanoparticles are not released to the medium in contact with microorganisms is the release of silver ions [47] and [48]. Moreover, it has been proposed that silver release due to the reaction with dissolved oxygen is the only mechanism explaining the antimicrobial activity of silver materials, either or not in nanoforms [49]. Copper and copper oxide materials also display considerable antimicrobial activity [50]. In the metal-containing particles used in this work, silver ( $\text{Ag}^0$ ) and copper ( $\text{CuO}$ ) were essentially included inside the mesoporous structure of SBA-15, which is in turn embedded in the polymer structure of the hybrid membranes. Therefore, the possibility of particle detaching and migration to the membrane surface was not realistic. Moreover, no silicon was found in ICP analyses of water and culture medium in contact with membranes. The damage produced by silver and copper ions to living cells has been shown to be primarily due oxidative stress followed by several associated impairments such as membrane damage or enzymatic dysfunction [15].

Many membrane modifications pursuing antibiofouling behavior have been proposed up to date. Most deal with surface modification with antimicrobials, mostly silver compounded or nanoparticles [51]. Park et al.

covalently immobilized silver nanoparticles after surface functionalization and found reduced irreversible biofouling and significant inhibition of bacterial growth [52]. However, and even if nanoparticles were not released from membrane surface due to their covalent attachment the loss of active metal was intense and almost 50% was loss during the initial filtration stages. Kim et al. attached silver containing macromolecules and showed that silver concentrations at membrane surface resulted in 85% reduction of the specific growth rate of *E. coli* [53]. Also, in this case a considerable amount of silver detached from membrane surface. In general, the issue of silver leaching during membrane fabrication and application has been recognized as critical. Moreover, in case of using metal salts, the leaching is highly dependent on the ion exchange with dissolved salts [54]. In contrast with surface-functionalization approaches, we used metal loaded particles with the active substances in reduced form as a way of reducing the rate of metal passing to the solution. We demonstrated that no nanoparticle leaching occurred and that a sustained release of metal ions is possible from their reduced forms, which can be easily dispersed in casting solutions without using complex functionalization procedures.

#### 4. Conclusions

Hybrid PES ultrafiltration membranes were prepared by incorporating mesostructured silica particles functionalized with silver, copper, and amine moieties. Composite membranes displayed asymmetric structure with relatively dense skin layer and a porous finger-like sublayer. The amount of surface pores significantly increased in doped membranes. All membranes were negatively charged and slightly hydrophobic with free energy of interaction slightly decreasing with the introduction of fillers.

The addition of particles increased permeability  $> 30\%$  in all cases, without reduction of membrane performance expressed as BSA rejection. The addition of mesoporous silica particles, functionalized or not, allowed fouling reduction up to 29% during protein filtration. All flow resistances were lower for composite membranes with respect to neat PES. The intrinsic membrane resistance was dominant suggesting that membrane permeation was limited by the inherent morphological characteristics of membranes.

Silver-loaded composites exhibited high antimicrobial activity, with complete removal of bacterial colonies either on membrane surface ( $< 1 \text{ CFU/cm}^2$ ) and in the liquid culture in contact with them ( $< 10 \text{ CFU/mL}$ ). The effect was lower, but also significant for copper-loaded materials. The antimicrobial action could be attributed to the release of metals, which diffused from loaded mesoporous silica and PES matrix to the bulk. The release of dissolved metals represented a 0.1–0.6% of the total content of metal of the tested membranes.

## Acknowledgements

Financial support for this work was provided by the FP7-ERA-Net Susfood, 2014/00153/001, the Spanish Ministry of Economy and Competitiveness, CTQ2014-57858-R and CTM2013-45775-C2-1-R and the Regional Government of Madrid through program S2013/MAE-2716-REMTAVARES-CM. BD thanks the University of Alcalá for the award of predoctoral grant.

## References

- [1] B. Chakrabarty, A.K. Ghoshal, M.K. Purkait, Ultrafiltration of stable oil-in-water emulsion by polysulfone membrane, *J. Memb. Sci.*, 325 (2008) 427-437.
- [2] P. Liu, V.R. Hill, D. Hahn, T.B. Johnson, Y. Pan, N. Jothikumar, C.L. Moe, Hollow-fiber ultrafiltration for simultaneous recovery of viruses, bacteria and parasites from reclaimed water, *J. Microbiol. Methods*, 88 (2012) 155-161.
- [3] K. Boussu, B. Van der Bruggen, A. Volodin, C. Van Haesendonck, J.A. Delcour, P. Van der Meeren, C. Vandecasteele, Characterization of commercial nanofiltration membranes and comparison with self-made polyethersulfone membranes, *Desalination*, 191 (2006) 245-253.
- [4] J.A. Prince, S. Bhuvana, K.V.K. Boodhoo, V. Anbharasi, G. Singh, Synthesis and characterization of PEG-Ag immobilized PES hollow fiber ultrafiltration membranes with long lasting antifouling properties, *J. Memb. Sci.*, 454 (2014) 538-548.
- [5] B. Van der Bruggen, Chemical modification of polyethersulfone nanofiltration membranes: A review, *J. Appl. Polym. Sci.*, 114 (2009) 630-642.
- [6] N. Maximous, G. Nakhla, W. Wan, Comparative assessment of hydrophobic and hydrophilic membrane fouling in wastewater applications, *J. Memb. Sci.*, 339 (2009) 93-99.
- [7] K.H. Choo, C.H. Lee, Understanding membrane fouling in terms of surface free energy changes, *J. Colloid. Interf. Sci.*, 226 (2000) 367-370.
- [8] L.J. Zhu, L.P. Zhu, J.H. Jiang, Z. Yi, Y.F. Zhao, B.K. Zhu, Y.Y. Xu, Hydrophilic and anti-fouling polyethersulfone ultrafiltration membranes with poly(2-hydroxyethyl methacrylate) grafted silica nanoparticles as additive, *J. Memb. Sci.*, 451 (2014) 157-168.
- [9] Y.F. Zhao, L.P. Zhu, Z. Yi, B.K. Zhu, Y.Y. Xu, Improving the hydrophilicity and fouling-resistance of polysulfone ultrafiltration membranes via surface zwitterionization mediated by polysulfone-based triblock copolymer additive, *J. Memb. Sci.*, 440 (2013) 40-47.
- [10] M.E. Shirtliff, J.T. Mader, A.K. Camper, Molecular interactions in biofilms, *Chem. Biol.*, 9 (2002) 859-871.
- [11] C.X. Liu, D.R. Zhang, Y. He, X.S. Zhao, R.B. Bai, Modification of membrane surface for anti-biofouling performance: Effect of anti-adhesion and anti-bacteria approaches, *J. Memb. Sci.*, 346 (2010) 121-130.
- [12] A. Rahimpour, S.S. Madaeni, Polyethersulfone (PES)/cellulose acetate phthalate (CAP) blend ultrafiltration membranes: Preparation, morphology, performance and antifouling properties, *J. Memb. Sci.*, 305 (2007) 299-312.
- [13] N. Akar, B. Asar, N. Dizge, I. Koyuncu, Investigation of characterization and biofouling properties of PES membrane containing selenium and copper nanoparticles, *J. Memb. Sci.*, 437 (2013) 216-226.
- [14] J.L. Hobman, L.C. Crossman, Bacterial antimicrobial metal ion resistance, *J. Med. Microbiol.*, 64 (2015) 471-497.
- [15] J.A. Lemire, J.J. Harrison, R.J. Turner, Antimicrobial activity of metals: mechanisms, molecular targets and applications, *Nat. Rev. Microbiol.*, 11 (2013) 371-384.
- [16] J.P. Ruparelia, A.K. Chatterjee, S.P. Duttagupta, S. Mukherji, Strain specificity in antimicrobial activity of silver and copper nanoparticles, *Acta Biomaterialia*, 4 (2008) 707-716.
- [17] M. Raffi, S. Mehrwan, T.M. Bhatti, J.I. Akhter, A. Hameed, W. Yawar, M.M. ul Hasan, Investigations into the antibacterial behavior of copper nanoparticles against *Escherichia coli*, *Ann. Microbiol.*, 60 (2010) 75-80.
- [18] J. Kim, B. Van der Bruggen, The use of nanoparticles in polymeric and ceramic membrane structures: Review of manufacturing procedures and performance improvement for water treatment, *Environ. Pollut.*, 158 (2010) 2335-2349.
- [19] S.B. Teli, S. Molina, A. Sotto, E. Garcia-Calvo, J. de Abajo, Fouling resistant polysulfone-PANI/TiO<sub>2</sub> ultrafiltration nanocomposite membranes, *Ind. Eng. Chem. Res.*, 52 (2013) 9470-9479.
- [20] J. Huang, K.S. Zhang, K. Wang, Z.L. Xie, B. Ladewig, H.T. Wang, Fabrication of polyethersulfone-mesoporous silica nanocomposite ultrafiltration membranes with antifouling properties, *J. Memb. Sci.*, 423 (2012) 362-370.
- [21] A. Martín, J.M. Arsuaga, N. Roldán, J. de Abajo, A. Martínez, A. Sotto, Enhanced ultrafiltration PES membranes doped with mesostructured functionalized silica particles, *Desalination*, 357 (2015) 16-25.
- [22] L.Y. Ng, A.W. Mohammad, C.P. Leo, N. Hilal, Polymeric membranes incorporated with metal/metal oxide nanoparticles: A comprehensive review, *Desalination*, 308 (2013) 15-33.
- [23] J. Quirós, S. Gonzalo, B. Jalvo, K. Boltes, J.A. Perdigón-Melón, R. Rosal, Electrospun cellulose acetate composites containing supported metal

- nanoparticles for antifungal membranes, *Sci. Total Environ.*, 563–564 (2016) 912-920.
- [24] D. Zhao, J. Feng, Q. Huo, N. Melosh, G.H. Fredrickson, B.F. Chmelka, G.D. Stucky, Triblock copolymer syntheses of mesoporous silica with periodic 50 to 300 angstrom pores, *Science*, 279 (1998) 548-552.
- [25] C.J. Van Oss, M.K. Chaudhury, R.J. Good, Interfacial Lifshitz-van der Waals and polar interactions in macroscopic systems, *Chem. Rev.*, 88 (1988) 927-941.
- [26] C.J. van Oss, Development and applications of the interfacial tension between water and organic or biological surfaces, *Colloids and Surfaces B: Biointerfaces*, 54 (2007) 2-9.
- [27] J. Lin, R. Zhang, W. Ye, N. Jullok, A. Sotto, B. Van der Bruggen, Nano-WS2 embedded PES membrane with improved fouling and permselectivity, *J. Colloid. Interf. Sci.*, 396 (2013) 120-128.
- [28] IOS 22196. Measurement of antibacterial activity on plastics and other nonporous surfaces, International Organization for Standardization, Geneva, Switzerland, (2011).
- [29] X.G. Wang, K.S.K. Lin, J.C.C. Chan, S.F. Cheng, Direct synthesis and catalytic applications of ordered large pore aminopropyl-functionalized SBA-15 mesoporous materials, *J. Phys. Chem. B*, 109 (2005) 1763-1769.
- [30] F.R. Rouquérol, J.; Sing, K.S.W., Applications of adsorption by porous solids, in: T.M. Lechter (Ed.) *Chemical Thermodynamics*, Blackwell, Cambridge, 2000, pp. 77-84.
- [31] M. Kruk, M. Jaroniec, S.H. Joo, R. Ryoo, Characterization of regular and plugged SBA-15 silicas by using adsorption and inverse carbon replication and explanation of the plug formation mechanism, *J. Phys. Chem. B*, 107 (2003) 2205-2213.
- [32] M. Choi, F. Kleitz, D.N. Liu, H.Y. Lee, W.S. Ahn, R. Ryoo, Controlled polymerization in mesoporous silica toward the design of organic-inorganic composite nanoporous materials, *J. Am. Chem. Soc.*, 127 (2005) 1924-1932.
- [33] G. Morales, R. van Grieken, A. Martín, F. Martínez, Sulfonated polystyrene-modified mesoporous organosilicas for acid-catalyzed processes, *Chem. Eng. J.*, 161 (2010) 388-396.
- [34] P. Aerts, I. Genne, S. Kuypers, R. Leysen, I.F.J. Vankelecom, P.A. Jacobs, Polysulfone-aerosil composite membranes Part 2. The influence of the addition of aerosil on the skin characteristics and membrane properties, *J. Memb. Sci.*, 178 (2000) 1-11.
- [35] A. Sotto, A. Boromand, R. Zhang, P. Luis, J.M. Arsuaga, J. Kim, B. Van der Bruggen, Effect of nanoparticle aggregation at low concentrations of TiO<sub>2</sub> on the hydrophilicity, morphology and fouling resistance of PES-TiO<sub>2</sub> membranes, *Abstracts of Papers of the American Chemical Society*, 243 (2012).
- [36] D.S. Wavhal, E.R. Fisher, Membrane surface modification by plasma-induced polymerization of acrylamide for improved surface properties and reduced protein fouling, *Langmuir*, 19 (2003) 79-85.
- [37] G.L. Jadav, P.S. Singh, Synthesis of novel silica-polyamide nanocomposite membrane with enhanced properties, *J. Memb. Sci.*, 328 (2009) 257-267.
- [38] W. Peng, I.C. Escobar, D.B. White, Effects of water chemistries and properties of membrane on the performance and fouling—A model development study, *J. Memb. Sci.*, 238 (2004) 33-46.
- [39] Y. Chang, M.M. Benjamin, Modeling formation of natural organic matter fouling layers on ultrafiltration membranes, *J. Environ. Eng.*, 129 (2003) 25-32.
- [40] T.J. Silhavy, D. Kahne, S. Walker, The bacterial cell envelope, *Cold Spring Harbor Perspectives in Biology*, 2 (2010) a000414.
- [41] M. Yasuyuki, K. Kunihiro, S. Kurissery, N. Kanavillil, Y. Sato, Y. Kikuchi, Antibacterial properties of nine pure metals: a laboratory study using *Staphylococcus aureus* and *Escherichia coli*, *Biofouling*, 26 (2010) 851-858.
- [42] S. Heß, C. Gallert, Growth behavior of *E. coli*, *Enterococcus* and *Staphylococcus* species in the presence and absence of sub-inhibitory antibiotic concentrations: consequences for interpretation of culture-based data, *Microbial Ecology*, 72 (2016) 898-908.
- [43] K. Hori, S. Matsumoto, Bacterial adhesion: From mechanism to control, *Biochem. Eng. J.*, 48 (2010) 424-434.
- [44] E. Klodzinska, M. Szumski, E. Dziubakiewicz, K. Hryniewicz, E. Skwarek, W. Janusz, B. Buszewski, Effect of zeta potential value on bacterial behavior during electrophoretic separation, *Electrophoresis*, 31 (2010) 1590-1596.
- [45] X. Tang, S.H. Flint, J.D. Brooks, R.J. Bennett, Factors affecting the attachment of microorganisms isolated from ultrafiltration and reverse osmosis membranes in dairy processing plants, *J. Appl. Microbiol.*, 107 (2009) 443-451.
- [46] Q. Zhao, Y. Liu, C. Wang, S. Wang, Evaluation of bacterial adhesion on Si-doped diamond-like carbon films, *Appl. Surf. Sci.*, 253 (2007) 7254-7259.
- [47] V.K. Sharma, K.M. Siskova, R. Zboril, J.L. Gardea-Torresdey, Organic-coated silver nanoparticles in biological and environmental conditions: Fate, stability and toxicity, *Adv. Colloid Interface Sci.*, 204 (2014) 15-34.
- [48] X. Yang, A.P. Gondikas, S.M. Marinakos, M. Auffan, J. Liu, H. Hsu-Kim, J.N. Meyer, Mechanism of silver nanoparticle toxicity is

- dependent on dissolved silver and surface coating in *caenorhabditis elegans*, Environ. Sci. Technol., 46 (2012) 1119-1127.
- [49] Z.M. Xiu, Q.B. Zhang, H.L. Puppala, V.L. Colvin, P.J.J. Alvarez, Negligible particle-specific antibacterial activity of silver nanoparticles, Nano Letters, 12 (2012) 4271-4275.
- [50] J. Ramyadevi, K. Jeyasubramanian, A. Marikani, G. Rajakumar, A.A. Rahuman, Synthesis and antimicrobial activity of copper nanoparticles, Mater. Letters, 71 (2012) 114-116.
- [51] I. Sawada, R. Fachrul, T. Ito, Y. Ohmukai, T. Maruyama, H. Matsuyama, Development of a hydrophilic polymer membrane containing silver nanoparticles with both organic antifouling and antibacterial properties, J. Memb. Sci., 387–388 (2012) 1-6.
- [52] S.Y. Park, J.W. Chung, Y.K. Chae, S.Y. Kwak, Amphiphilic thiol functional linker mediated sustainable anti-biofouling ultrafiltration nanocomposite comprising a silver nanoparticles and poly(vinylidene fluoride) membrane, ACS Appl. Mater. Interfaces, 5 (2013) 10705-10714.
- [53] Y. Kim, D. Rana, T. Matsuura, W.J. Chung, Towards antibiofouling ultrafiltration membranes by blending silver containing surface modifying macromolecules, Chem. Commun., 48 (2012) 693-695.
- [54] J. Mansouri, T. Charlton, V. Chen, T. Weiss, Biofouling performance of silver-based PES ultrafiltration membranes, Desal. and Water Treat., (2016) 1-15.

# Supplementary Material

## Fouling and biofouling resistance of metal-doped mesostructured silica/polyethersulfone ultrafiltration membranes

Berta Díez<sup>1</sup>, Nuria Roldán<sup>2</sup>, Antonio Martín<sup>2</sup>, Arcadio Sotto<sup>2</sup>, José Antonio Perdigón-Melón<sup>1</sup>, Jesús Arsuaga<sup>2,\*</sup>, Roberto Rosal<sup>1,\*</sup>

1 Department of Chemical Engineering, University of Alcalá, E-28871 Alcalá de Henares, Madrid, Spain

2 School of Experimental Science and Technology, ESCET, Rey Juan Carlos University, E-28933, Móstoles, Madrid, Spain

\* Corresponding authors: [jesusmaria.arsuaga@urjc.es](mailto:jesusmaria.arsuaga@urjc.es), [roberto.rosal@uah.es](mailto:roberto.rosal@uah.es)

**Table S1.** Textural properties of particles.

**Table S2.** Membrane surface  $\zeta$ -potential, contact angle measurements and surface free energy components.

**Experimental.** Derivation of surface hydrophobicity from contact angle values.

**Figure S1.** Low angle XRD patterns of pure SBA-15 and functionalized materials.

**Figure S2.** Nitrogen adsorption-desorption isotherms of SBA-15 and functionalized materials.

**Figure S3.** TEM micrographs of (a) SBA-15, (b) Cu/SBA-15, (c) Ag/SBA-15 and (d) Triamine/SBA-15.

**Figure S4.** BSA rejection of manufactured membranes for 1 g/L BSA aqueous solutions at 2 bar TMP.

**Figure S5.** Microbial colonization of membranes exposed to *S. aureus* cultures (20 h, 36 °C). PES (A), AgSBA@PES (B), TriSBA@PES (C) and AgTriSBA@PES (D).

**Figure S6.** Microbial colonization of TriSBA@PES membranes exposed to *E. coli* (A-B-C) and *S. aureus* (D-E-F) for 20 h at 36 °C. The different magnifications show irregular colonization patterns and biofilm formation.

**Figure S7.** Live/dead confocal micrographs of *E. coli* cultured on (A) PES, (B) CuSBA@PES, (C) AgSBA@PES, (D) TriSBA@PES, (E) CuTriSBA@PES and (F) AgTriSBA@PES.

**Figure S8.** Live/dead confocal micrographs of *S. aureus* cultured on (A) PES, (B) CuSBA@PES, (C) AgSBA@PES, (D) TriSBA@PES, (E) CuTriSBA@PES and (F) AgTriSBA@PES.

**Figure S9.** ICP-MS analyses of permeate from AgSBA@PES and CuSBA@PES before (solid lines) and after (dashed lines) 5 kDa ultrafiltration of membrane permeate. Error bars show no significant differences for silver (in grey) and copper (in blue).

**Table S1.** Textural properties of particles.

Sample	$S_{BET}$ (m <sup>2</sup> /g)	$V_t^a$ (cm <sup>3</sup> /g)	$D_p^a$ (nm)	Particle size <sup>b</sup> (μm)
SBA-15	675	1.06	8.0	1.4 ± 0.2
Cu/SBA-15	589	1.00	8.0	1.5 ± 0.4
Ag/SBA-15	549	0.95	7.9	1.5 ± 0.2
Triamine/SBA-15	481	0.68	7.0	2.2 ± 1.0

<sup>a</sup> Total pore volume and pore size calculated by BJH method from the adsorption branch of the N<sub>2</sub> isotherm.

<sup>b</sup> Measured in NMP (polymer solvent).

**Table S2.** Membrane surface ζ-potential, contact angle measurements and surface free energy components.

Material	ζ-potential	Contact angle (°)			Surface free energy components (mJ/m <sup>2</sup> )					
	(mV)	Water	Glycerol	Diiodomethane	$\gamma_S^{LW}$	$\gamma_S^+$	$\gamma_S^-$	$\gamma_S^{AB}$	$\gamma_S$	$\Delta G_{SLS}$
PES	-42.6 ± 4.0	65.2 ± 0.4	58.5 ± 2.2	20.8 ± 0.5	47.5	0.04	12.3	1.5	49.0	-39.8
SBA@PES	-36.6 ± 6.1	64.8 ± 0.6	61.8 ± 3.2	36.4 ± 2.8	41.4	0.06	15.6	1.9	43.2	-27.3
TriSBA@PES	-31.9 ± 1.2	64.1 ± 1.8	62.7 ± 1.5	42.8 ± 0.4	38.2	0.10	17.6	2.6	40.8	-20.8
AgSBA@PES	-47.6 ± 5.7	64.2 ± 0.7	61.9 ± 1.2	31.0 ± 0.8	43.8	0.05	16.1	0.6	44.3	-28.2
CuSBA@PES	-43.7 ± 0.1	65.1 ± 1.7	62.2 ± 0.3	38.6 ± 2.7	40.3	0.07	15.7	2.1	42.5	-26.5
AgTriSBA@PES	-32.5 ± 4.8	64.3 ± 1.0	62.3 ± 0.7	36.2 ± 2.3	41.5	0.03	16.6	1.4	42.8	-25.4
CuTriSBA@PES	-28.3 ± 2.7	66.3 ± 1.6	62.5 ± 1.8	33.7 ± 0.3	42.6	0.03	14.2	1.2	43.9	-32.0
<i>E.coli</i>	-	16.7 ± 1.3	44.0 ± 3.5	58.7 ± 0.5	29.3	1.1	62.0	16.3	45.6	+44.2
<i>S.aureus</i>	-	25.8 ± 3.1	38.3 ± 2.8	56.7 ± 2.6	40.4	0.8	45.6	11.9	52.3	+22.6

**Experimental.** Derivation of surface hydrophobicity from contact angle values.

The Lifshitz–van der Waals (LW), electron donor (–) and electron acceptor (+) components of the surface tension were estimated from CA values for water, glycerol and diiodomethane according to the following expression in which  $\theta$  are the pure liquid contact angles [1]:

$$(1 + \cos \theta) \gamma_L = 2 \left( \sqrt{\gamma_S^{LW} \gamma_L^{LW}} + \sqrt{\gamma_S^+ \gamma_L^-} + \sqrt{\gamma_S^- \gamma_L^+} \right) \quad (1)$$

In this approach, the total surface free energy ( $\gamma_S$ ) is the sum of the non-polar London-van der Waals component ( $\gamma_S^{LW}$ ) and the acid-base component ( $\gamma_S^{AB}$ ), which in turn comprises two non-additive parameters: the electron-acceptor ( $\gamma_S^+$ ) and the electron-donor ( $\gamma_S^-$ ) surface tension parameters:

$$\gamma_S = \gamma_S^{LW} + \gamma_S^{AB} = \gamma_S^{LW} + 2 \sqrt{\gamma_S^+ \gamma_S^-} \quad (2)$$

The three components of the solid free surface energy,  $\gamma_S^{LW}$ ,  $\gamma_S^+$  and  $\gamma_S^-$  are unknowns that can be solved by measuring the CA with three liquids taking into account that the components of the liquid free surface energy,  $\gamma_L^{LW}$ ,  $\gamma_L^+$  and  $\gamma_L^-$  for the probe liquids are available in the literature for a number of pure substances [2]. According to Van Oss, the total interfacial tension between the solid film and water,  $\gamma_{SL}$ , can be expressed as follows [3]:

$$\gamma_{SL} = \left( \sqrt{\gamma_S^{LW}} - \sqrt{\gamma_L^{LW}} \right)^2 + 2 \left( \sqrt{\gamma_S^+ \gamma_S^-} + \sqrt{\gamma_L^+ \gamma_L^-} - \sqrt{\gamma_S^+ \gamma_L^-} - \sqrt{\gamma_L^+ \gamma_S^-} \right) \quad (3)$$

The free energy of interaction between two identical condensed phases immersed gives a direct measure of their hydrophobicity and can be derived from  $\gamma_{SL}$ :

$$\Delta G_{SLS} = -2 \gamma_{SL} \quad (4)$$

$\Delta G_{SLS}$  gives a measure of the hydrophobicity or hydrophilicity of the surface. If  $\Delta G_{SLS} > 0$ , the surface is hydrophilic, and if  $\Delta G_{SLS} < 0$ , it is hydrophobic.

[1] C.J. Van Oss, M.K. Chaudhury, R.J. Good, Interfacial Lifshitz-van der Waals and polar interactions in macroscopic systems, *Chem. Rev.*, 88 (1988) 927-941.

[2] A. Holländer, On the selection of test liquids for the evaluation of acid-base properties of solid surfaces by contact angle goniometry. *J. Colloid Interface Sci.*, 169 (1995) 493-496.

[3] C.J. van Oss, Development and applications of the interfacial tension between water and organic or biological surfaces, *Colloids Surf B: Biointerfaces*, 54 (2007) 2-9.

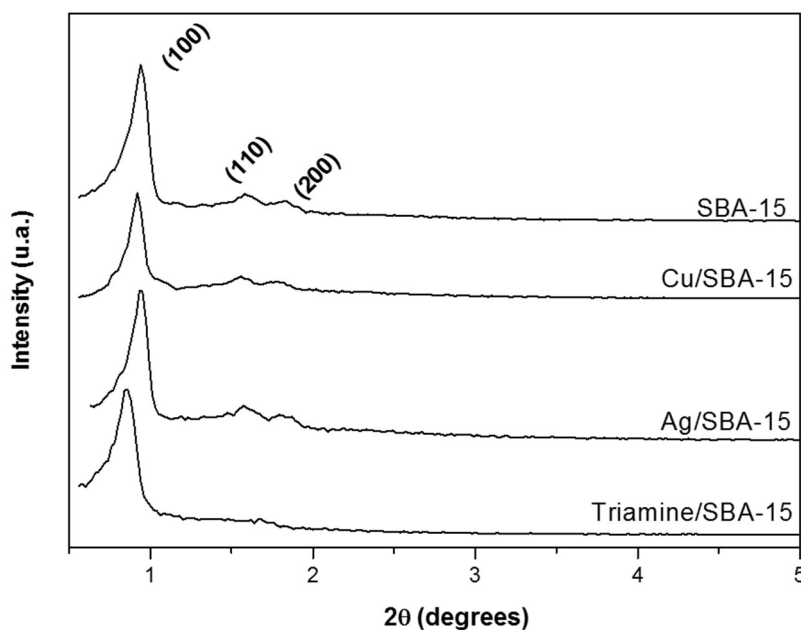


**Fig. S1.** Low angle XRD patterns of pure SBA-15 and functionalized materials.

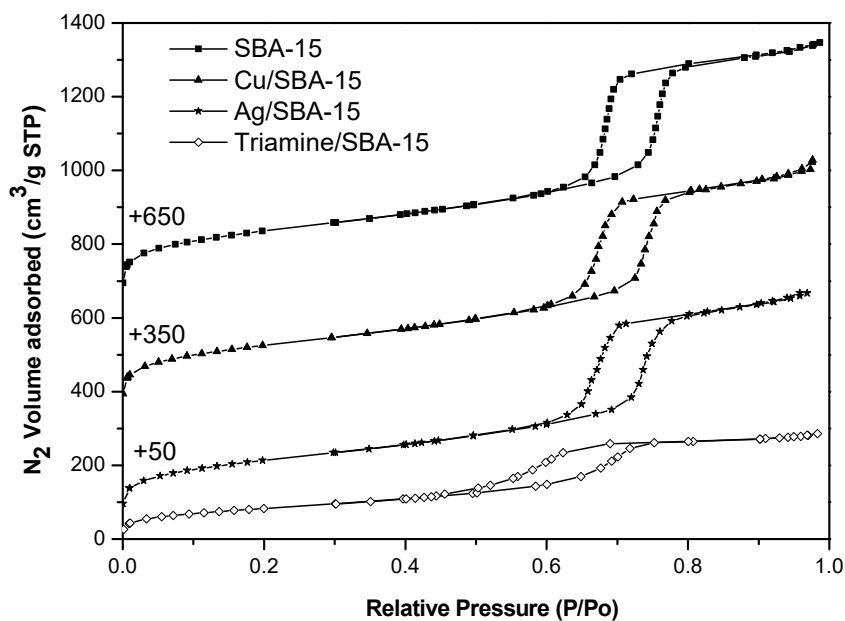


**Fig. S2.** Nitrogen adsorption-desorption isotherms of SBA-15 and functionalized materials.

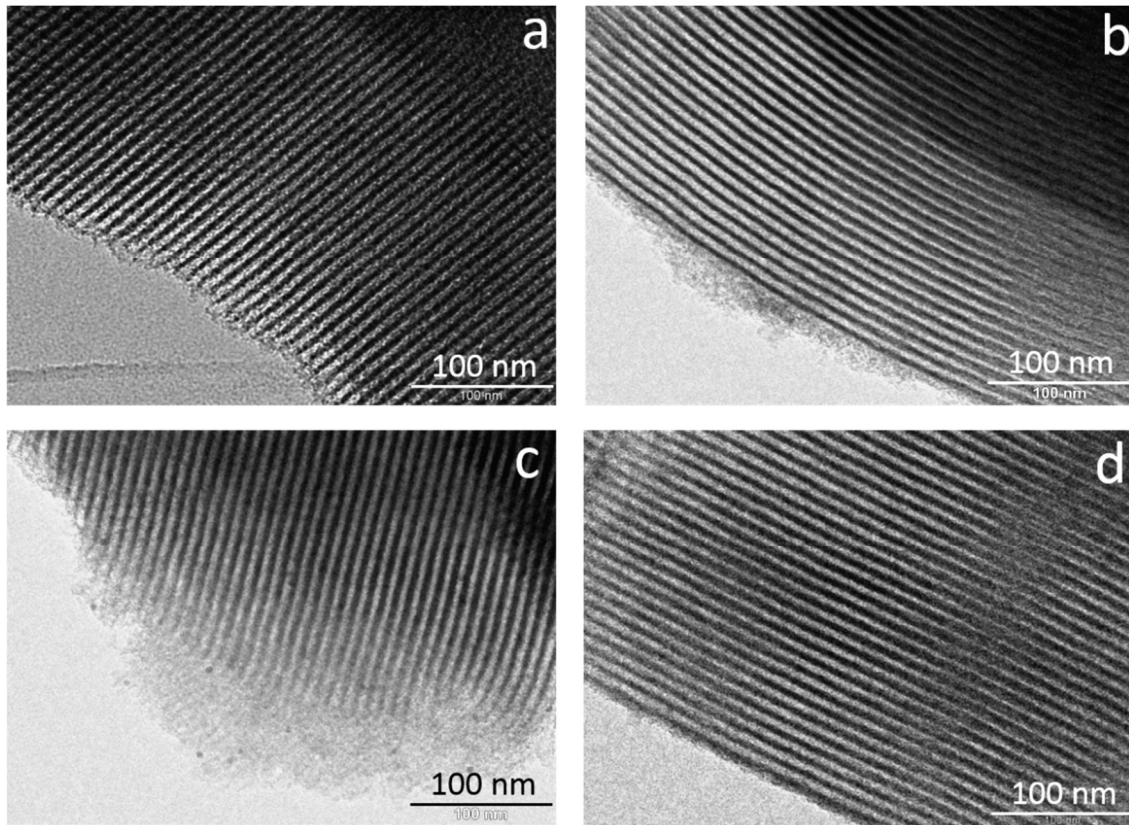


**Fig. S3.** TEM micrographs of (a) SBA-15, (b) Cu/SBA-15, (c) Ag/SBA-15 and (d) Triamine/SBA-15.

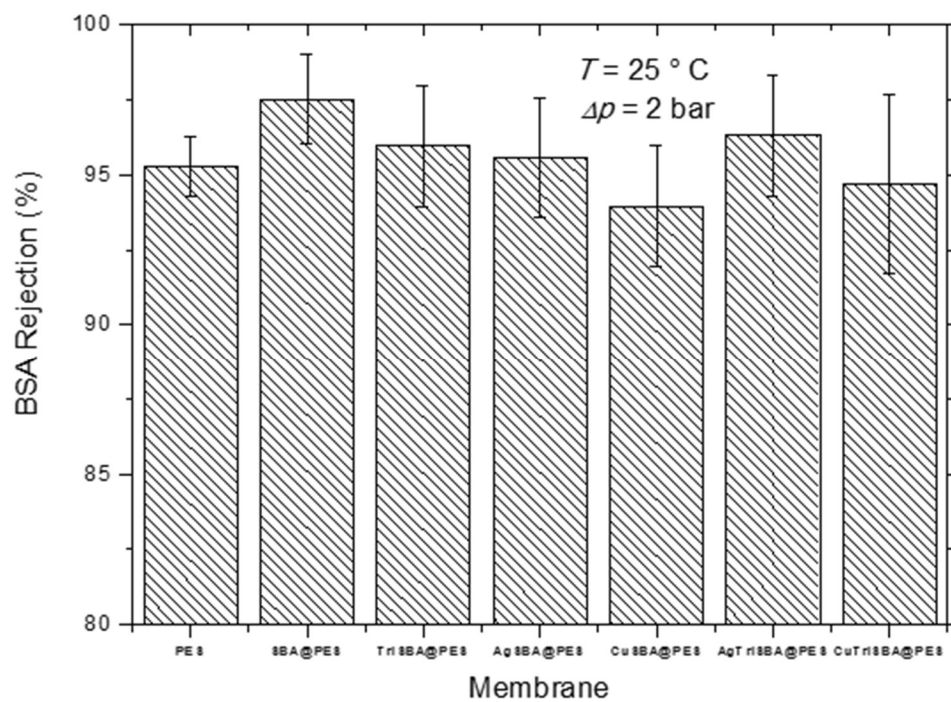


**Fig. S4.** BSA rejection of manufactured membranes for 1 g/L BSA aqueous solutions at 2 bar TMP.

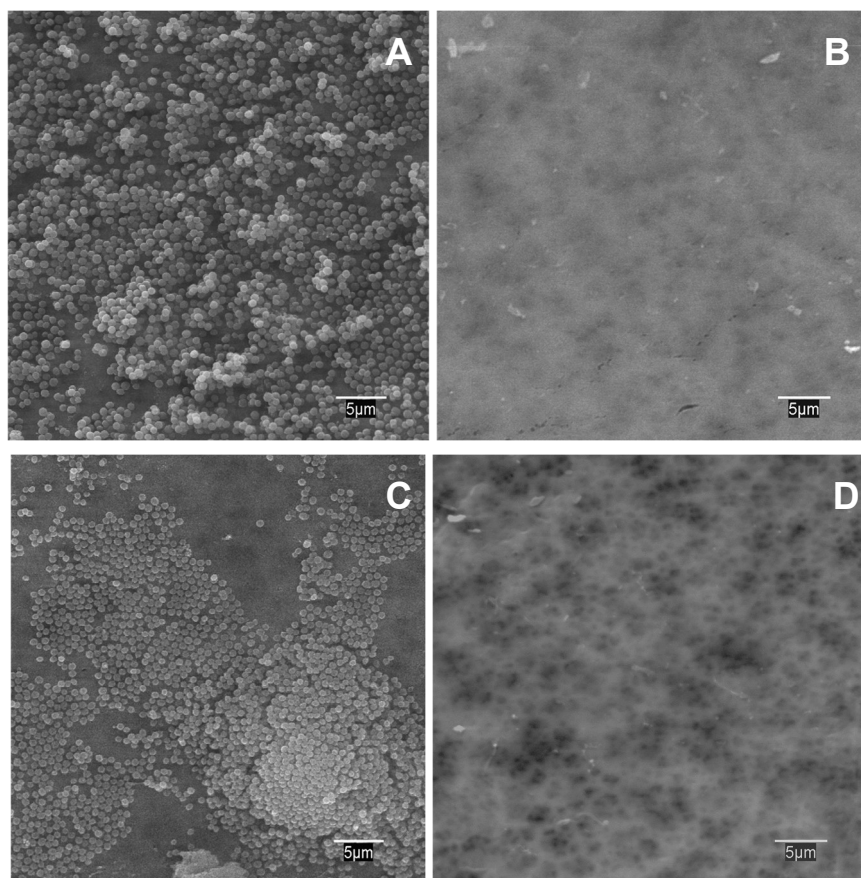


**Fig. S5.** Microbial colonization of membranes exposed to *S. aureus* cultures (20 h, 36 °C). PES (A), AgSBA@PES (B), TriSBA@PES (C) and AgTriSBA@PES (D).

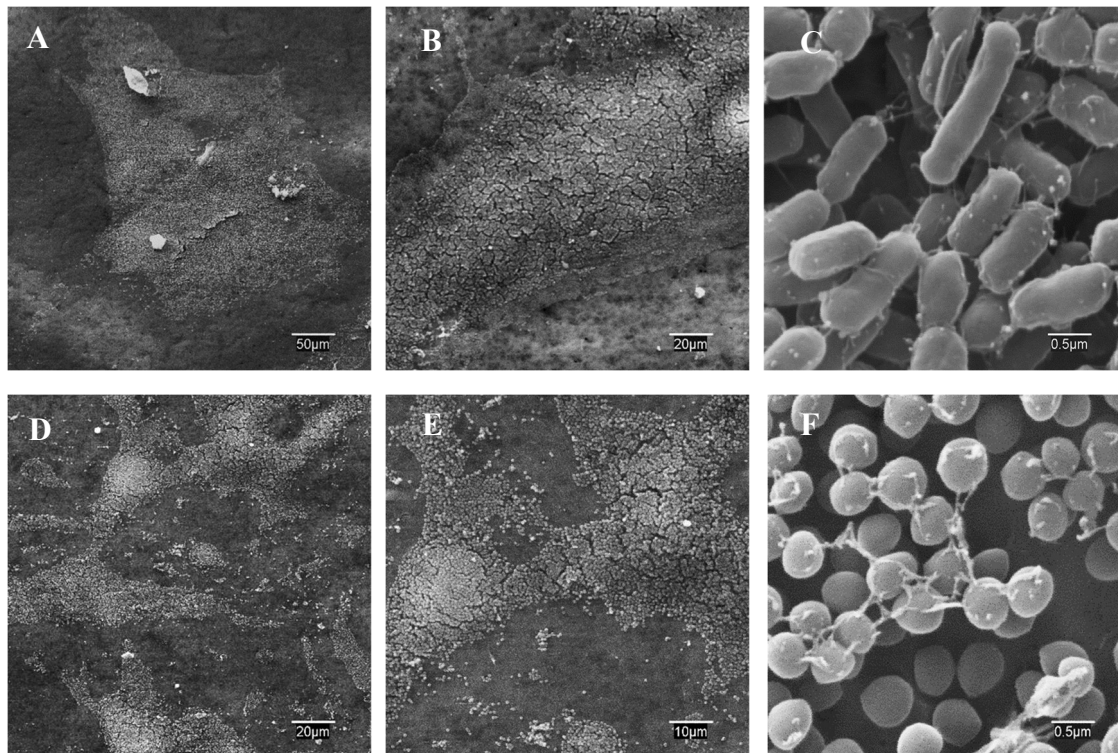


**Fig. S6.** Microbial colonization of TriSBA@PES membranes exposed to *E. coli* (A-B-C) and *S. aureus* (D-E-F) for 20 h at 36 °C. The different magnifications show irregular colonization patterns and biofilm formation.

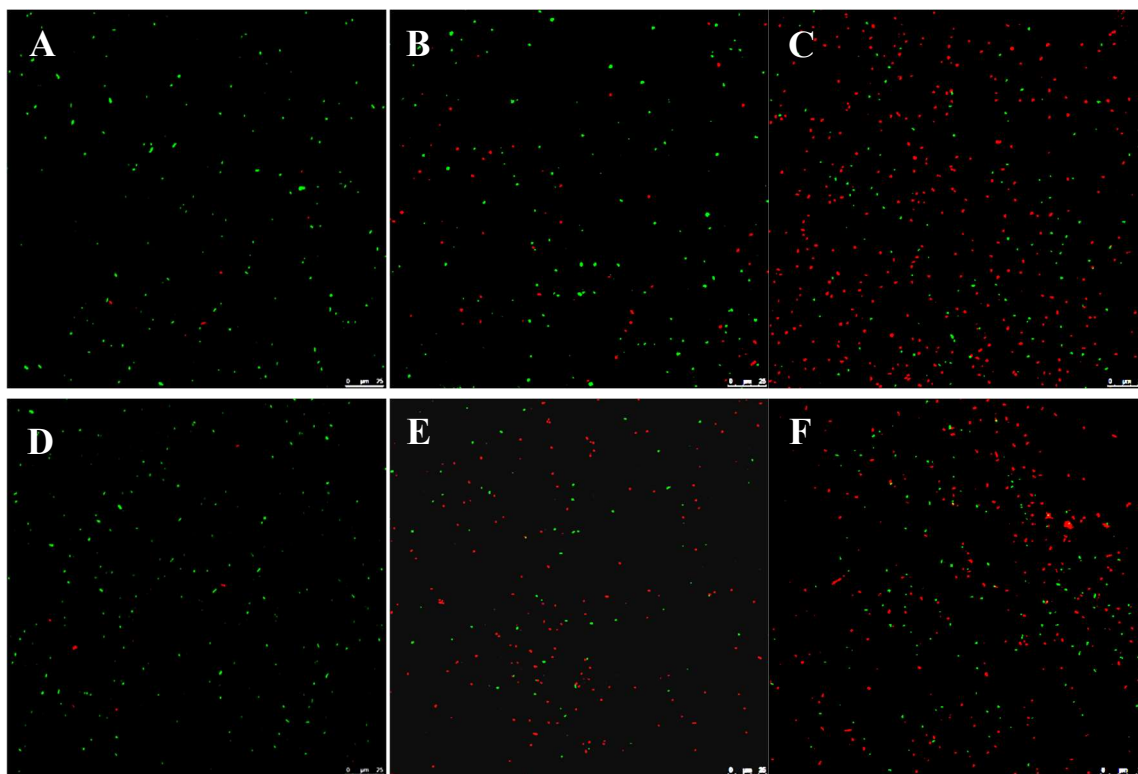


**Fig. S7.** Live/dead confocal micrographs of *E. coli* cultured on (A) PES, (B) CuSBA@PES, (C) AgSBA@PES, (D) TriSBA@PES, (E) CuTriSBA@PES and (F) AgTriSBA@PES.

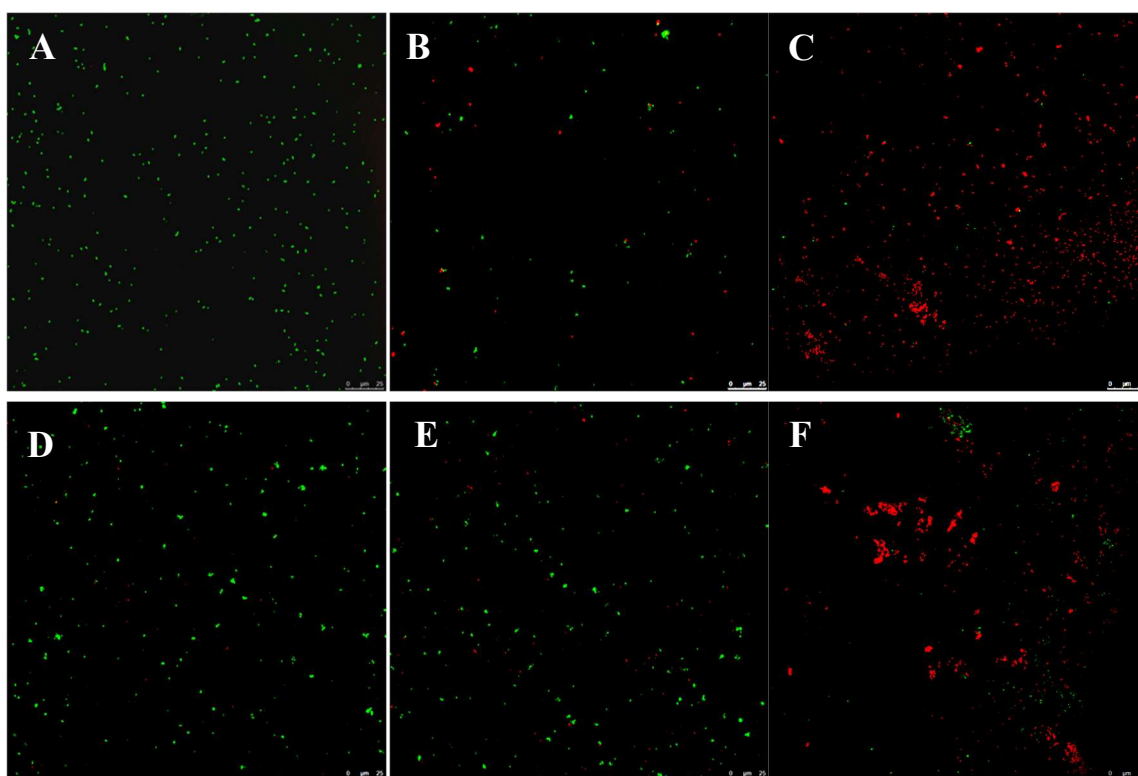


**Fig. S8.** Live/dead confocal micrographs of *S. aureus* cultured on (A) PES, (B) CuSBA@PES, (C) AgSBA@PES, (D) TriSBA@PES, (E) CuTriSBA@PES and (F) AgTriSBA@PES.

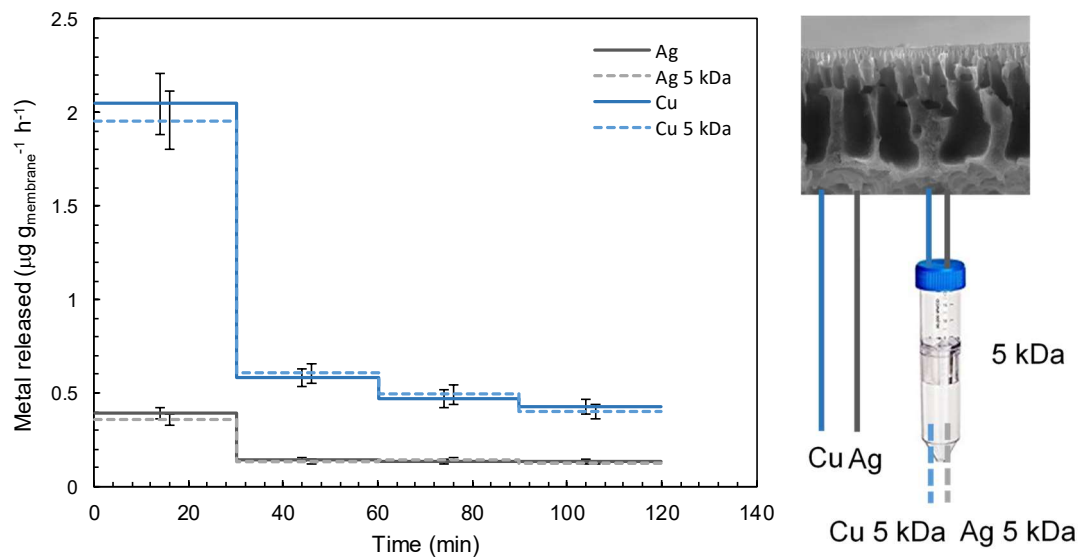


**Figure S9.** ICP-MS analyses of permeate from AgSBA@PES and CuSBA@PES before (solid lines) and after (dashed lines) 5 kDa ultrafiltration of membrane permeate. Error bars show no significant differences for silver (in grey) and copper (in blue).